Editors' Suggestion

Coherent Dynamics of Molecular Vibrations in Single Plasmonic Nanogaps

Fiona Bell, Lukas Jakob, Caleb Todd, Ishaan Lohia, Yeeun Roh, Rakesh Arul,* and Jeremy J. Baumberg†
NanoPhotonics Centre, Cavendish Laboratory, Department of Physics, JJ Thompson Avenue, University of Cambridge, Cambridge CB3 0US, United Kingdom

(Received 31 March 2025; revised 25 June 2025; accepted 15 July 2025; published 15 August 2025)

Coupling with a resonant optical cavity is well known to modify the coherence of molecular vibrations. However, in the case of molecules coupled to a plasmonic nanocavity mode, the local mechanisms of vibrational coherence decay remain unclear. Here, the dynamics of a few hundred molecules of nitrothiophenol (NTP) within a single plasmonic nanocavity are studied by sum-frequency generation. Time-resolved experiments reveal a coherence lifetime sensitive to intermolecular dipole coupling strength, and is found to compete with cavity-induced vibrational dephasing above a threshold $\sim$10 cm^{-1}. Tuning of the system dipole strength presents a quantitative means to explore the energy landscape of coherent interactions within nanoscale vibrational platforms, relevant for studies from vibrational chemistry to cavity quantum optomechanics.

DOI: 10.1103/txdw-nqvn

Molecular vibrational coherence plays a key role in processes ranging from coherent photosynthesis [1] to the nonradiative decay of emitters. [2] Such vibrational coherences can normally only be manipulated by changing the molecule or by coupling to resonant optical cavities. Plasmonic nanocavity geometries, which confine light to the deep subwavelength regime [3], exhibit extreme field enhancements and light-matter interactions (accessing single vibrational bonds) [4]. Controlling the vibrational coherence of plasmonic cavity-molecule systems would impact catalysis, [5] quantum optics [6,7], and photodetection [8,9].

The coherence of excited vibrations is limited by phase memory loss due to both population decay and pure dephasing, the latter being highly sensitive to molecule-substrate and inter-molecular interactions. At metallic interfaces, ultrafast studies report coherence lifetimes of a few picoseconds for molecule-metal coupled systems [10–13]. However, this has been little studied in nanocavities [14–16], so mechanisms for coherence loss of tightly confined molecules in intense highly localized optical fields remain unclear.

Lateral interactions between molecules have been observed in some cases to extend the lifetime of coherently excited states [17]. For vibrations of polar bonds, intermolecular coupling arises from dipole-dipole interactions between the permanent infrared dipoles of neighboring molecules. When closely packed together, these vibrations hybridize to form a band with modes delocalized over many molecules [18,19]. In the infrared spectrum, this is identified by characteristic energy shifts and splitting of the dressed vibration when compared to the individual uncoupled molecules [20–22]. Collective vibrational motion has also been observed at visible frequencies within plasmonic nanogap geometries, where plasmon-induced coupling of Raman-active vibrations arises via mediation of intermolecular interactions by localized cavity modes [23]. A recent optomechanical framework describes this behavior [24–26], experimentally verified by the observation of laser-induced vibrational pumping [27], linewidth broadening, and frequency shifts [28] of vibrational modes.

Here, ultrafast time-resolved sum-frequency generation (SFG) is used to study the influence of collective motion on vibrational dephasing within plasmonic nanogaps. Molecules are directly excited via absorption of a midinfrared (MIR) ps pulse. Subsequent scattering of a Raman probe pulse upconverts this signal to the visible, producing a spectro-temporal map of the dephasing dynamics. Plasmonic enhancement of both visible and MIR fields within the $\sim$1 nm nanogap cavity is achieved using a dual-wavelength nanoparticle-on-resonator (NPoR) geometry [Fig. 1(a)] [8]. This enables detection of the coherent signal from a single nanogap structure containing only a few hundred molecules of nitrothiophenol (NTP). Owing to its high binding affinity to gold, NTP forms well-ordered self-assembled monolayers (SAMs) which support vibrational modes with simultaneous MIR and Raman activity. The NO_2 stretch mode (ν_{NO_2} = 1340 cm^{-1}) has a strong permanent dipole moment which is ideal to study visible-MIR nonlinear mixing [29,30]. In tightly packed SAMs, the vibration shows strong

*Contact author: ra554@cam.ac.uk
†Contact author: jjb12@cam.ac.uk

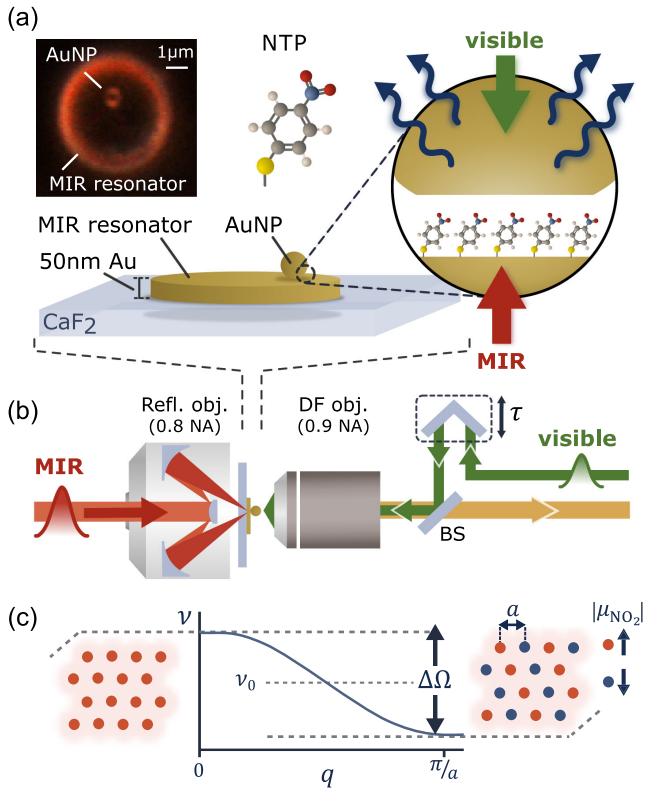

FIG. 1. (a) Nanoparticle-on-resonator nanocavity comprised of midinfrared disk resonator, nitrothiophenol molecular monolayer, and gold nanoparticle on calcium fluoride substrate. Inset: darkfield scattering image of single NPoR. (b) Experimental setup with variable delay time τ between visible and MIR pulses. Reflective objective focuses MIR through the substrate while DF objective focuses the visible Raman beam and collects scattered signal, separated by the beam splitter (BS) and dispersed by spectrometer onto CCD. (c) Illustrative phonon dispersion for lattice of coupled vibrations with separation a and dipole moment μ_{NO_2}. In-phase mode (lattice momentum $q = 0$) is split from out-of-phase vibration ($q = \pi/a$) by frequency $\Delta\Omega$.

dipole-dipole interactions causing an energy shift of the mode, observed in both infrared [31] and Raman spectra [32].

By temporally resolving the SFG signal, we measure the dephasing dynamics of the nitrostretch vibration and extract a maximum dipole coupling strength of $\Delta\Omega = 18 \pm 1\ \mathrm{cm}^{-1}$. Tuning the strength of this coupling modifies the dynamics of the delocalized vibration, with pronounced motional-narrowing-induced dipolar interactions. We observe a transition from a regime in which vibrational dynamics are dictated by intermolecular coupling, to an energy landscape where cavity effects dominate coherence loss. An experimental estimation of the corresponding optomechanical coupling strength yields $2g_{\mathrm{opt}} \sim 13\ \mathrm{cm}^{-1}$ (Supplemental Material [33] Sec. S8.2). The comparable energy scale of these interactions demonstrates the competition between these two dephasing mechanisms and the importance of considering cavity interactions in the design of coherent devices.

The spatial overlap and enhancement of both infrared and visible fields is realized using a well-characterized nanoparticle-on-resonator geometry [Fig. 1(a)]. A self-assembled molecular monolayer (SAM) of NTP is formed on the surface of a gold microdisk (diameter 5 μm, thickness 50 nm) that supports resonances at MIR wavelengths [8]. Drop casting of 80 nm gold nanoparticles (NPs) subsequently forms a plasmonic nanogap geometry (gap size 1.3 nm) showing resonances in the visible region. Molecules within the dual-wavelength resonator experience > 200 fold enhancement of both visible and MIR fields enabling nonlinear mixing (even under continuous wave illumination) [8]. Surface-enhanced Raman scattering (SERS) spectra of molecules in individual NPoRs are measured using a custom-built microscope [Fig. 1(b)]. A tunable MIR ultrashort pulse ($\lambda_{\mathrm{MIR}} = 5$–$12$ μm, duration ~ 2 ps) is focused from below using a reflective objective. A coaligned high-NA objective focuses a visible laser ($\lambda_{\mathrm{vis}} = 785$ nm, pulse duration ~ 2 ps) with variable relative delay time τ onto the sample. Nanoparticles are located using wide-angle darkfield (DF) scattering imaging [inset, Fig. 1(a)]. The backscattered SERS and nonlinear mixing signals are collected and dispersed by a spectrometer onto a CCD camera.

The collective behavior of static dipoles within an ordered molecular monolayer is modeled as vibrational oscillators coupled together by nearest-neighbor Coulomb interactions. The vibrational modes of many tightly packed uniformly oriented molecules hybridize to form a band of collective vibrations with a frequency splitting $\Delta\Omega$ determined by the average interaction strength [Fig. 1(c)]. The energy of the collective modes is shifted with respect to the unperturbed frequency ν_0 of an isolated molecule. The interaction potential $\hat{V}_{ij}$ between two dipole moments $\boldsymbol{\mu}_i, \boldsymbol{\mu}_j$, at lattice positions $\boldsymbol{r}_i, \boldsymbol{r}_j$ is defined as

$$\hat{V}_{ij} = \frac{\boldsymbol{\mu}_i \cdot \boldsymbol{\mu}_j - 3(\boldsymbol{\mu}_i \cdot \boldsymbol{r}_{ij})(\boldsymbol{\mu}_j \cdot \boldsymbol{r}_{ij})}{4\pi\varepsilon_0 |\boldsymbol{r}_{ij}|^3} - V_{ij}^{\mathrm{im}}, \qquad (1)$$

where $\boldsymbol{r}_{ij}$ is the dipole separation and ε_0 the vacuum permittivity. The image potential V_{ij}^{im} includes interaction terms that account for screening via image dipoles [32] induced via proximity to the free electrons in the two metal interfaces surrounding the nanogap. The frequency eigenstates forming the cooperative band are calculated from the resulting interaction matrix.

For a lattice with a single-molecule unit cell, symmetry dictates that only modes comprised of in-phase vibrations yield a net dipole moment. However, a nonvanishing dipole moment for the antisymmetric out-of-phase vibration can appear if the unit cell is comprised of two or more translationally inequivalent molecules. Phenol-based molecules that undergo self-assembly on metal surfaces

typically form a hexagonal ($\sqrt{3} \times \sqrt{3}$) herringbone structure [34] in which the in-plane rotation ϕ alternates sign for every other molecule. A further tilt angle θ relative to the surface normal is also present, arising from the metal-thiol bond. The coupling of ~350 NTP molecules is thus modeled as a hexagonal arrangement of dipoles with lattice constant $a = 0.5$ nm, dipole moment $|\mu_{NO_2}| = 0.27$ D [26], in a herringbone orientation defined by the angles $\phi = 30°$ and $\theta = 30°$. Calculation of the symmetric $(++)$ and antisymmetric $(+-)$ mode energies gives a predicted splitting of $\Delta\Omega = 16.1\ \mathrm{cm}^{-1}$ (Supplemental Material [33] Sec. S2).

The dephasing dynamics of the collective NO_2 vibration is measured by time-resolved SFG [Fig. 2(a)]. The incident MIR field $E_{\mathrm{MIR}}(t)$, resonantly tuned to the energy of the vibrational $|\mathrm{v}\rangle_{0\to1}$ transition, induces a time-dependent first-order polarization $P^{(1)}(t)$. This contains information on the molecular vibrational response function $R_{\mathrm{mol}}(t)$, which decays on a timescale defined by the coherent dephasing time T_2. In the limit of purely homogeneous broadening, the line shape of vibrational modes is assumed to be Lorentzian and the total dephasing time determined by the population decay time T_1 and pure dephasing time T_2^* as $T_2^{-1} = (2T_1)^{-1} + (T_2^*)^{-1}$ [35]. The vibrational response of n vibrational modes of frequencies ω_n, amplitudes A_n, phases ϕ_n and linewidths $\Gamma_n = 1/T_{2,n}$ is given by

$$R_{\mathrm{mol}}(t) = A_{NR} e^{i\phi_{NR}} + \sum_n A_n e^{-t/T_{2,n}} e^{-i(\omega_n t + \phi_n)}, \quad (2)$$

where A_{NR}, ϕ_{NR} respectively correspond to the amplitude and relative phase of the vibrationally nonresonant component of the response [36,37]. Scattering via a visible field $E_{vis}(t)$ subsequently upconverts this signal to a second order polarisation $P^{(2)}(t,\tau)$ with an intensity $|P^{(2)}(t,\tau)|^2 \propto |E_{\mathrm{vis}}(t-\tau) * [E_{\mathrm{MIR}}(t) * R_{\mathrm{mol}}(t)]|^2$, whose time integral is directly related to the intensity of the SFG signal.

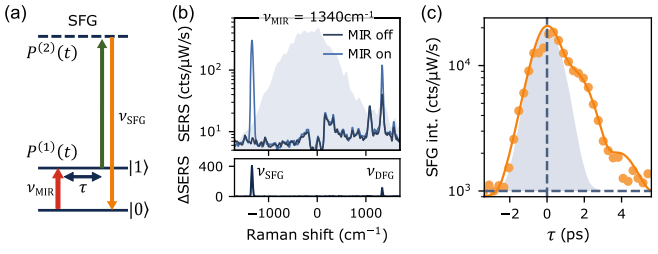

FIG. 2. (a) Excitation scheme of sum-frequency generation. (b) SERS intensities, and difference spectrum (ΔSERS); blue shaded area is DF scattering spectrum. Induced peaks when MIR laser is on corresponds to sum- or difference-frequency generation at $\nu_{\mathrm{SFG/DFG}} = \pm\nu_{\mathrm{MIR}}$. (c) Time-resolved integrated SFG intensity with fit to the 2-Lorentzian model (orange line). Gaussian system response of 1.01 ± 0.04 ps (blue shaded).

At zero delay time, the nonlinear response of the NTP NPoR [Fig. 2(b)] shows two induced components at Raman shifts $\mp\nu_{\mathrm{MIR}}$, corresponding to scattering processes with energy equal to the sum and difference of visible and MIR fields. Tuning ν_{MIR} across the NO_2 vibration (Supplemental Material [33] Fig. S6) demonstrates a negligible contribution to the SFG intensity from non-resonant components (subsequently ignored). Scanning τ produces a spectro-temporal map from which the coherent dynamics of the vibrationally excited state is extracted from the integrated SFG intensity. For the 16 individual NPoR structures measured, fitting each decay to $R_{\mathrm{mol}}(t)$ with a single Lorentzian mode yields an average dephasing time $\bar{T}_2 = 2.1 \pm 0.1$ ps ($\bar{\Gamma}_2 = 2.6 \pm 0.1\ \mathrm{cm}^{-1}$).

Further inspection reveals an oscillating modulation of the SFG intensity (clearly visible for ~25% of particles) [Fig. 2(c)]. This beating signal is characteristic of the interference between two coherent vibrations. A fit of the data using Eq. (2) with two vibrational modes $n = 1, 2$ separated by frequency $\Delta\Omega = \omega_2 - \omega_1$ gives a beat frequency of $16 \pm 1\ \mathrm{cm}^{-1}$. This is in excellent agreement with the splitting between delocalized symmetric $(++)$ and antisymmetric $(+-)$ modes estimated from the dipole-dipole coupling model above. No additional modes are present in the solution IR and Raman spectrum of NTP that could account for this interference, and we note that the appearance of this beating is unique to the NPoR structure. An equivalent measurement of ~700 nanogaps in an aggregated monolayer of gold NPs [38] does not reproduce the effect (Supplemental Material [33] Fig. S7), which we attribute to a distribution of nanogaps and molecular arrangements averaging out collective behaviors.

The effect of delocalization on vibrational dephasing is studied by varying the dipole-dipole coupling strength between NO_2 groups. A nonpolar spacer molecule 1,1'-biphenol-4-thiol (BPT) is partially substituted within the NTP SAM, thus tuning the average dipole separation [Fig. 3(a)]. The fractional surface coverage of NTP molecules x_n is extracted from high-resolution CW SERS spectra by the intensity ratio of NTP ($1570\ \mathrm{cm}^{-1}$) and BPT ($1585\ \mathrm{cm}^{-1}, 1600\ \mathrm{cm}^{-1}$) ring mode vibrations [Fig. 3(f)]. Samples with increasing dilution of NTP are measured, at average fractional coverages of $\bar{x}_n = 0.73$ ($N = 16$) and 0.55 ($N = 13$), with ~30% giving clear oscillations.

The coherent dephasing of delocalized vibrations can also be extracted for decreasing intermolecular coupling. Substituting BPT within the NPoR does not shift the MIR resonance, so the cavity-enhanced population decay time T_1 should remain constant. A narrow distribution of dephasing times is observed for NTP-only SAMs [$\bar{x}_n = 0.97$, Fig. 4(a)]. In contrast, at mean fractional coverage $\bar{x}_n = 0.73$ both a systematic decrease in dephasing times (to average $\bar{T}_2 = 1.8 \pm 0.1$ ps) and a broadening of the overall distribution are seen. The first is characteristic of "motional narrowing," previously reported in similar

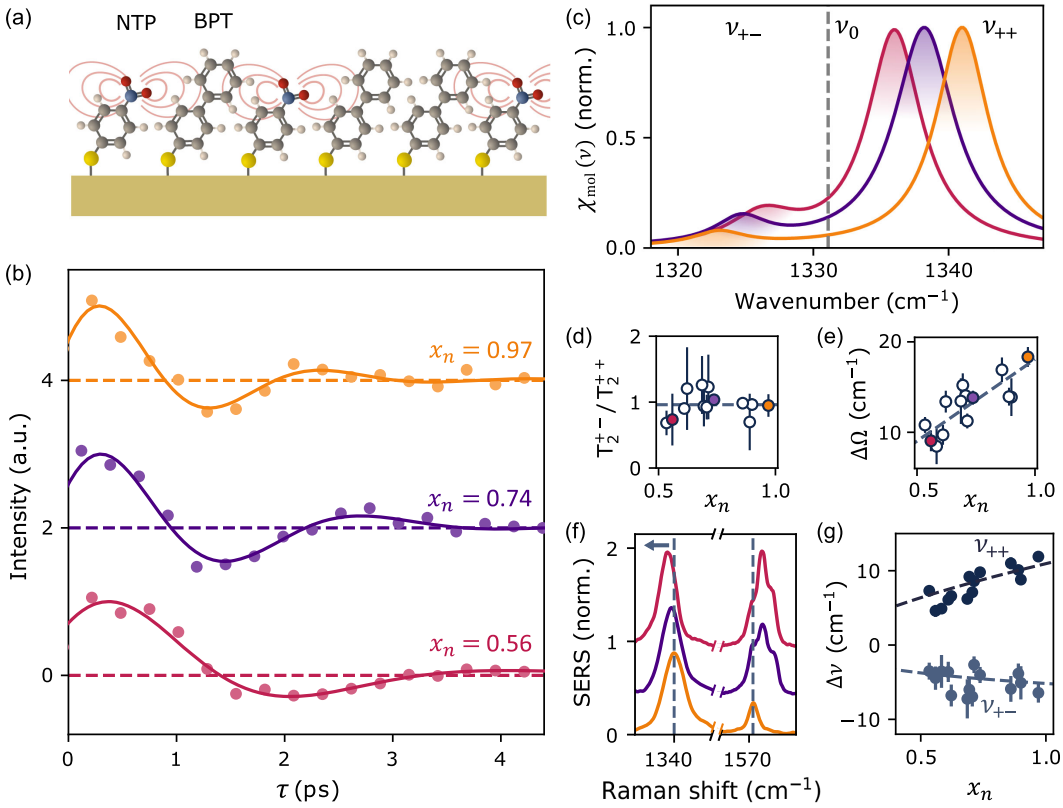

FIG. 3. (a) Separating dipoles by diluting NTP with BPT, giving fractional surface coverage x_n. (b) Oscillatory component of measured decay for representative NPoRs at each x_n, extracted from 2-Lorentzian fit by subtracting a single exponential decay. (c) Normalized frequency-domain molecular response $\chi_{mol}(\nu)$ from (b). Fill-fraction dependence of (d) T_2 ratio and (e) $\Delta\Omega$ between $(++)$ and $(+-)$ modes, with linear fits (dashed). Data from (b),(c) indicated in corresponding colours. (f) Normalized CW SERS intensity of NTP-BPT mixed SAM vs x_n. Symmetric mode of NO_2 vibration blueshifts (arrow) with increasing dipole coupling strength whilst frequency of ring vibration at 1570 cm^{-1} remains constant. CW spectral collected at average laser intensity of 18 μW μm^{-2}. (g) Wavenumber shift $\Delta\nu$ of coupled modes vs fractional coverage. Dashed lines are expected shifts from dipole-dipole coupling model.

delocalised vibrational systems [39]. This can be understood within a picture where vibrations "hop" between molecules on a timescale $\propto \Delta\Omega^{-1}$. If this occurs at a rate faster than pure dephasing induces phase loss, the coherence is protected to an extent dictated by the degree of delocalization. Within this description, we expect $T_2 \propto \Delta\Omega$ [40]. Using the tuning relation in Fig. 3(e) gives the ratio $\Delta\Omega(\bar{x}_n = 0.73)/\Delta\Omega(\bar{x}_n = 0.97) = 0.77$, comparable to the ratio of dephasing times $\bar{T}_2(\bar{x}_n = 0.73)/\bar{T}_2(\bar{x}_n = 0.97) = 0.85$.

Decreasing the NTP fractional coverage to $\bar{x}_n = 0.55$, further broadens the range of measured dephasing times [Fig. 4(a)]. Coherent oscillations persist, thus excluding vibrational localization effects. We suggest this transition comes from energy exchange mechanisms in such plasmonic systems. Above a threshold $\Delta\Omega_t \sim 10$ cm^{-1}, dipole-dipole interactions dominate, evidenced by motional narrowing of the vibrational dephasing rate. However, as the distance between dipoles increases and the strength of this coupling reduces, a different mechanism of energy exchange dominates dephasing dynamics.

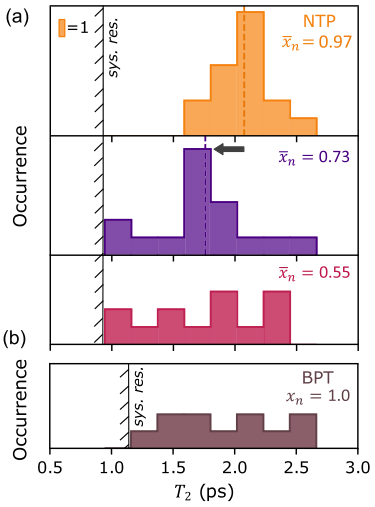

FIG. 4. Distribution of measured dephasing times for (a) NTP-BPT mixed SAMs vs NTP fractional coverage and (b) BPT-only SAM. Scale indicated used for all plots. System resolution indicated for each MIR frequency.

To understand the origin of dephasing for small dipole-dipole interactions, a comparison without dipole-dipole coupling is made by measuring BPT-only SAMs. The coupled ring vibration at 1585 cm^{-1} has an IR cross section approximately tenfold weaker than the NO_2 vibration of NTP [41] with negligible intermolecular coupling. Consequently, the vibration shows no frequency shift when tuning the average molecular separation [Fig. 3(f)]. Inserting appropriate parameters into our model of dipole-dipole coupling predicts mode splitting of $\Delta\Omega = 1.6$ cm^{-1} (Supplemental Material [33] Sec. S8.3). Tuning the MIR frequency to the 1585 cm^{-1} vibration of BPT (without varying pulse intensity), the time-dependent SFG intensity is extracted for 13 NPs (Supplemental Material [33] Fig. S11).

The distribution of dephasing times is determined using the single Lorentzian fit of Eq. (2) [Fig. 4(b)]. Despite its weak infrared coupling strength, the measured T_2 of the coupled ring mode shows a similar behavior to the nitro-stretch vibration from the $\bar{x}_n = 0.55$ NTP-BPT mixed SAM, lying within a broad range bounded by the system resolution. This suggests that excitation of vibrations within a plasmonic nanogap geometry inherently gives rise to a wide range of possible dephasing times. This intriguing result suggests that the atomic details of molecule-metal configuration drastically change the dephasing rates.

Recent experiments in other nanogap systems have demonstrated a coherence lifetime sensitive to the local cavity environment, with an accelerated dephasing time for increasing optical field strength [14,15]. A broad distribution of lifetimes therefore can arise from variations between individual nanocavities, originating from specific NP geometry [42], local SAM uniformity [43], and the heterogeneous optical field within each nanocavity [44,45]. We therefore propose that the observed drastic narrowing of measured NTP dephasing times [Fig. 4(a)] shows the transition to a regime where lateral dipole interactions dominate over the cavity-molecule coupling strength, i.e., $\Delta\Omega > 2g_{\mathrm{opt}}$. Here, vibrational delocalization plays a critical role in mitigating dephasing, even in the presence of structural disorder and optical field variations. This condition is never met for BPT [27], and cavity interactions dominate even for the pure SAM. In an optomechanical picture, g_{opt} is expected to have a $\sqrt{x_n}$ dependence, while our measurements show $\Delta\Omega$ to be linear with x_n. Therefore, above the threshold coupling strength, where $\Delta\Omega \approx 2g_{\mathrm{opt}}$, dipole-dipole interactions will always dominate (Supplemental Material [33] Sec. S8.4). Extrapolating to a complete monolayer of NTP gives $2g_{\mathrm{opt}} \sim 13$ cm^{-1}, comparable to the value predicted for our system (Supplemental Material [33] Sec. S8.2).

In conclusion, plasmonic enhancement of visible-MIR nonlinear processes within single nanocavities reveals the local dephasing dynamics of a few hundred tightly confined molecules. Dipole-dipole coupling between neighboring molecules delocalizes the vibrations of the system. Interference between in-phase and out-of-phase collective vibrations is observed as coherent beating. The competition between intermolecular dipole-dipole coupling and local cavity-molecule interactions controls vibrational dephasing rates. Above a threshold coupling strength $\Delta\Omega_t > 10\,cm^{-1}$, dipolar interactions extend the coherence lifetime by ~200% and reduce variations induced by plasmonic coupling that normally obscure dephasing dynamics. The effects observed are applicable to a wide range of molecules [46,47] and solid-state dipoles [48,49] spanning across MIR and THz spectral regimes. Control of vibrational coherences in metal-molecule systems opens possibilities for testing the role of collective vibrations on optomechanical cooling [50], optoelectronics, and energy transfer [2], as well as plasmonic catalysis [51], where collective dynamics can strongly influence reaction pathways.

Acknowledgments—We acknowledge support from EPSRC Grants No. MIRVALS EP/Y008162/1, No. MIRVID EP/Y036379/1, No. UbOHT EP/X037770/1, and ERC Grant No. PICOFORCE 883703. F. B. acknowledges support from EPSRC Award No. 2437572. R. A. acknowledges support from St. John's College Cambridge, and the Winton Programme for the Physics of Sustainability. I. L. acknowledges support from the Harding Scholars programme. C. T. acknowledges support from the Gates Cambridge Foundation.

The authors declare no competing financial interest.

Data availability—The data that support the findings of this Letter are openly available [52].

[1] S. R. Rather, G. D. Scholes, and L. X. Chen, From coherence to function: Exploring the connection in chemical systems, Acc. Chem. Res. **57**, 2620 (2024).
[2] P. Ghosh *et al.*, Decoupling excitons from high-frequency vibrations in organic molecules, Nature (London) **629**, 355 (2024).
[3] J. J. Baumberg, J. Aizpurua, M. H. Mikkelsen, and D. R. Smith, Extreme nanophotonics from ultrathin metallic gaps, Nat. Mater. **18**, 668 (2019).
[4] C. Carnegie *et al.*, Room-temperature optical picocavities below 1 nm 3 accessing single-atom geometries, J. Phys. Chem. Lett. **9**, 7146 (2018).
[5] Z. Zhang, C. Zhang, H. Zheng, and H. Xu, Plasmon-driven catalysis on molecules and nanomaterials, Acc. Chem. Res. **52**, 2506 (2019).
[6] V. Pouthier, Vibrational exciton mediated quantum state transfer: Simple model, Phys. Rev. B **85**, 214303 (2012).
[7] S. T. Velez, K. Seibold, N. Kipfer, M. D. Anderson, V. Sudhir, and C. Galland, Preparation and decay of a single quantum of vibration at ambient conditions, Phys. Rev. X **9**, 041007 (2019).

[8] A. Xomalis, X. Zheng, R. Chikkaraddy, Z. Koczor-Benda, E. Miele, E. Rosta, G. A. E. Vandenbosch, A. Martínez, and J. J. Baumberg, Detecting mid-infrared light by molecular frequency upconversion in dual-wavelength nanoantennas, Science **374**, 1268 (2021).

[9] W. Chen *et al.*, Continuous-wave frequency upconversion with a molecular optomechanical nanocavity, Science **374**, 1264 (2021).

[10] A. L. Harris, L. Rothberg, L. Dhar, N. J. Levinos, and L. H. Dubois, Vibrational energy relaxation of a polyatomic adsorbate on a metal surface: Methyl thiolate (CH3S) on Ag(111), J. Chem. Phys. **94**, 2438 (1991).

[11] C. Matranga and P. Guyot-Sionnest, Vibrational relaxation of cyanide at the metal/electrolyte interface, J. Chem. Phys. **112**, 7615 (2000).

[12] W. G. Roeterdink, O. Berg, and M. Bonn, Frequency- and time-domain femtosecond vibrational sum frequency generation from CO adsorbed on Pt(111), J. Chem. Phys. **121**, 10174 (2004).

[13] H. S. AlSalem and S. P. K. Koehler, Ultrafast vibrational dephasing times of modified graphene, J. Phys. Chem. C **126**, 7571 (2022).

[14] L. A. Jakob, W. M. Deacon, R. Arul, B. De Nijs, N. S. Mueller, and J. J. Baumberg, Accelerated molecular vibrational decay and suppressed electronic nonlinearities in plasmonic cavities through coherent Raman scattering, Phys. Rev. B **109**, 195404 (2024).

[15] X. Zheng, Q. Pei, J. Tan, S. Bai, Y. Luo, and S. Ye, Local electric field in nanocavities dictates the vibrational relaxation dynamics of interfacial molecules, Chem. Sci. **15**, 11507 (2024).

[16] R. Wilcken, J. Nishida, J. F. Triana, A. John-Herpin, H. Altug, S. Sharma, F. Herrera, and M. B. Raschke, Antenna-coupled infrared nanospectroscopy of intramolecular vibrational interaction, Proc. Natl. Acad. Sci. U.S.A. **120**, e2220852120 (2023).

[17] W. G. Roeterdink, O. Berg, and M. Bonn, Frequency- and time-domain femtosecond vibrational sum frequency generation from CO adsorbed on Pt(111), J. Chem. Phys. **121**, 10174 (2004).

[18] B. N. J. Persson and R. Ryberg, Vibrational interaction between molecules adsorbed on a metal surface: The dipole-dipole interaction, Phys. Rev. B **24**, 6954 (1981).

[19] A. V. Snigur and V. M. Rozenbaum, Davydov splitting of vibrational spectra of adsorbates, Opt. Spectrosc. **95**, 685 (2003).

[20] J. A. Lau, A. M. Schönemann, D. Schwarzer, A. M. Wodtke, J. A. Lau, and A. M. Wodtke, The coverage dependence of the infrared absorption of CO adsorbed to NaCl(100), J. Chem. Phys. **153** (2020).

[21] J. Heidberg, E. Kampshoff, and M. Suhren, Correlation field, structure, and phase transition in the monolayer CO adsorbed on NaCl(100) as revealed from polarization Fourier-transform infrared spectroscopy, J. Chem. Phys. **95**, 9408 (1991).

[22] F. M. Hoffmann, Infrared reflection-absorption spectroscopy of adsorbed molecules, Surf. Sci. Rep. **3**, 107 (1983).

[23] Y. Zhang, J. Aizpurua, and R. Esteban, Optomechanical collective effects in surface-enhanced Raman scattering from many molecules, ACS Photonics **7**, 1676 (2020).

[24] P. Roelli, C. Galland, N. Piro, and T. J. Kippenberg, Molecular cavity optomechanics as a theory of plasmon-enhanced Raman scattering, Nat. Nanotechnol. **11**, 164 (2016).

[25] R. Esteban, J. J. Baumberg, and J. Aizpurua, Molecular optomechanics approach to surface-enhanced Raman scattering, Acc. Chem. Res. **55**, 1889 (2022).

[26] P. Roelli, H. Hu, E. Verhagen, S. Reich, and C. Galland, Nanocavities for molecular optomechanics: Their fundamental description and applications, ACS Photonics **11** (2024).

[27] A. Lombardi, M. K. Schmidt, L. Weller, W. M. Deacon, F. Benz, B. De Nijs, J. Aizpurua, and J. J. Baumberg, Pulsed molecular optomechanics in plasmonic nanocavities: From nonlinear vibrationalinstabilities to bond-breaking, Phys. Rev. X **8**, 1 (2018).

[28] L. A. Jakob *et al.*, Giant optomechanical spring effect in plasmonic nano- and picocavities probed by surface-enhanced Raman scattering, Nat. Commun. **14**, 1 (2023).

[29] M. Linke, M. Hille, M. Lackner, L. Schumacher, S. Schlücker, and E. Hasselbrink, Plasmonic effects of Au nanoparticles on the vibrational sum frequency spectrum of 4-nitrothiophenol, J. Phys. Chem. C **123**, 24234 (2019).

[30] F. Cecchet, D. Lis, J. Guthmuller, B. Champagne, G. Fonder, Z. Mekhalif, Y. Caudano, A. A. Mani, P. A. Thiry, and A. Peremans, Theoretical calculations and experimental measurements of the vibrational response of p-NTP SAMs: An orientational analysis, J. Phys. Chem. C **114**, 4106 (2010).

[31] T. P. Gray, J. Nishida, S. C. Johnson, and M. B. Raschke, 2D vibrational exciton nanoimaging of domain formation in self-assembled monolayers, Nano Lett. **21**, 5754 (2021).

[32] N. S. Mueller, R. Arul, L. A. Jakob, M. O. Blunt, T. Földes, E. Rosta, and J. J. Baumberg, Collective mid-infrared vibrations in surface-enhanced Raman scattering, Nano Lett. **22**, 7254 (2022).

[33] See Supplemental Material at http://link.aps.org/supplemental/10.1103/txdw-nqvn for experimental methods, microscope characterization, and CW SERS spectra of mixed SAMs, along with details of the theoretical dipole coupling model, fitting procedure of measured decays, and estimation of the cavity coupling strength.

[34] J. Nara, S. Higai, Y. Morikawa, and T. Ohno, Adsorption structure of benzenethiol on Au(1 1 1): First-principles study, Appl. Surf. Sci. **237**, 434 (2004).

[35] A. Laubereau and W. Kaiser, Vibrational dynamics of liquids and solids investigated by picosecond light pulses, Rev. Mod. Phys. **50**, 607 (1978).

[36] J. M. Marmolejos, P. J. Bisson, and M. J. Shultz, Gold as a standard phase reference in complex sum frequency generation measurements, J. Chem. Phys. **150**, 124705 (2019).

[37] W. Guo, B. Liu, Y. He, E. You, Y. Zhang, S. Huang, J. Wang, and Z. Wang, Plasmonic gold nanohole arrays for surface-enhanced sum frequency generation detection, Nanomater. Nanotechnol. **10**, 2557 (2020).

[38] R. Arul, D.-B. Grys, R. Chikkaraddy, N. S. Mueller, A. Xomalis, E. Miele, T. G. Euser, and J. J. Baumberg, Giant mid-IR resonant coupling to molecular vibrations in sub-nm

gaps of plasmonic multilayer metafilms, Light Sci. Appl. **11**, 281 (2022).
[39] B. N. J. Persson and R. Ryberg, Dipole-coupling-induced line narrowing in adsorbate vibrational spectroscopy, Chem. Phys. Lett. **174**, 443 (1990).
[40] B. N. J. Persson, F. M. Hoffmann, and R. Ryberg, Influence of exciton motion on the shape of optical absorption lines: Applications to vibrations at surfaces, Phys. Rev. B **34**, 2266 (1986).
[41] M. Oftadeh, S. Naseh, and M. Hamadanian, Electronic properties and dipole polarizability of thiophene and thiophenol derivatives via density functional theory, Comput. Theor. Chem. **966**, 20 (2011).
[42] E. Elliott, K. Bedingfield, J. Huang, S. Hu, B. de Nijs, A. Demetriadou, and J. J. Baumberg, Fingerprinting the hidden facets of plasmonic nanocavities, ACS Photonics **9**, 2643 (2022).
[43] J. U. Nielsen, M. J. Esplandiu, and D. M. Kolb, 4-Nitrothiophenol SAM on Au(111) investigated by *in situ* STM, electrochemistry, and XPS, Langmuir **17**, 3454 (2001).
[44] S. A. Lee and S. Link, Chemical interface damping of surface plasmon resonances, Acc. Chem. Res. **54**, 1950 (2021).
[45] W. Zhu, R. Esteban, A. G. Borisov, J. J. Baumberg, P. Nordlander, H. J. Lezec, J. Aizpurua, and K. B. Crozier, Quantum mechanical effects in plasmonic structures with subnanometre gaps, Nat. Commun. **7**, 11495 (2016).
[46] T. A. Ageeva, A. A. Bush, D. V. Golubev, A. S. Gorshkova, K. E. Kamentsev, O. I. Koifman, V. D. Rumyantseva, A. S. Sigov, and V. V. Fomichev, Porphyrin metal complexes with a large dipole moment, J. Organomet. Chem. **922**, 121355 (2020).
[47] T. N. Olney, N. M. Cann, G. Cooper, and C. E. Brion, Absolute scale determination for photoabsorption spectra and the calculation of molecular properties using dipole sum-rules, Chem. Phys. **223**, 58 (1997).
[48] S. A. Blanton, R. L. Leheny, M. A. Hines, and P. Guyot-Sionnest, Dielectric dispersion measurements of CdSe nanocrystal colloids: Observation of a permanent dipole moment, Phys. Rev. Lett. **79**, 865 (1997).
[49] H. Xu *et al.*, Dipole–dipole-interaction-assisted self-assembly of quantum dots for highly efficient light-emitting diodes, Nat. Photonics **18**, 186 (2024).
[50] L. A. Jakob, A. Juan-Delgado, N. S. Mueller, S. Hu, R. Arul, R. A. Boto, R. Esteban, J. Aizpurua, and J. J. Baumberg, Optomechanical pumping of collective molecular vibrations in plasmonic nanocavities, ACS Nano **19**, 10977 (2025).
[51] J. Jeong, H.-H. Shin, and Z. H. Kim, Unveiling the mechanism of plasmon photocatalysis via multiquantum vibrational excitation, ACS Nano **18**, 25290 (2024).
[52] 10.17863/CAM.120068.